Anode-pore tortuosity in solid oxide fuel cells found from gas and current flow rates

V. Hugo Schmidt[*], Chih-Long Tsai

Department of Physics, EPS 264, Montana State University, Bozeman, MT 59717, USA

Abstract

The effect of solid oxide fuel cell (SOFC) anode thickness, porosity, pore size, and pore tortuosity on fuel and exhaust gas flow is calculated. Also determined is the concentration of these gases and of diluent gases as a function of position across the anode. The calculation is based on the dusty-gas model which includes a Knudsen (molecule–wall) collision term in the Stefan–Maxwell equation which is based on unlike-molecule collisions. Commonly made approximations are avoided in order to obtain more exact results. One such approximation is the assumption of uniform total gas pressure across the anode. Another such approximation is the assumption of zero fuel gas concentration at the anode–electrolyte interface under the anode saturation condition for which the SOFC output voltage goes to zero. Elimination of this approximation requires use of a model we developed (published elsewhere) for terminal voltage V as a function of electrolyte current density i. Key formulae from this model are presented. The formulae developed herein for gas flow and tortuosity are applied to the results of a series of careful experiments performed by another group, who used binary and ternary gas mixtures on the anode side of an SOFC. Our values for tortuosity are in a physically reasonable low range, from 1.7 to 3.3. They are in fair agreement with those obtained by the other group, once a difference in nomenclature is taken into account. This difference consists in their definition of tortuosity being what some call tortuosity factor, which is the square of what we and some others call tortuosity. The results emphasize the need for careful design of anode pore structures, especially in anode-supported SOFCs which require thicker anodes.
© 2008 Elsevier B.V. All rights reserved.

Keywords: Solid oxide fuel cells; Anode-supported; Tortuosity; Dusty-gas model; Gas flow

1. Introduction

Solid oxide fuel cells (SOFCs) provide efficient generation of electricity using a variety of fuels. They produce only steam exhaust if hydrogen is the fuel. The same device can act as a steam electrolyzer to produce hydrogen and oxygen from steam if a dc voltage is applied.

Present SOFCs operate in the 800–1000 °C (1073–1273 K) range, but strong efforts are in progress to extend this range downward to 600 °C (873 K) or lower to minimize interconnect cost by allowing use of stainless steel, and to reduce problems associated with thermal expansion, atomic migration, and corrosion. The main obstacle for this temperature reduction is the rapid decrease in solid electrolyte oxygen ion conductivity with decreasing temperature. Accordingly, the electrolyte is made as thin as possible, of order 10 μm. This requires that an electrode layer, usually the anode, must be made thick enough to mechanically support the cell.

With a thicker anode, one must calculate carefully the fuel and exhaust gas concentrations at the anode–electrolyte interface. These concentrations (or corresponding partial pressures) strongly affect $V(i)$, the terminal voltage V as a function of electrolyte current density i. The anode characteristics (assuming a much thinner cathode) also under some conditions determine the maximum attainable i. This is the current density when the fuel flow rate is high enough to reduce the fuel gas partial pressure at the interface to near zero, and the SOFC output voltage to exactly zero. This fuel pressure gradient in the anode is increased by the inflowing fuel molecule collisions with the outflowing exhaust molecules.

---

[*] Corresponding author. Tel.: +1 406 994 6173; fax: +1 406 994 4452.
E-mail addresses: schmidt@physics.montana.edu, tsai@physics.montana.edu (V.H. Schmidt).

Table 1
Tortuosities calculated for H_2/H_2O and CO/CO_2 binary systems

Fuel	p.p. (atm)	i_{as} (A cm^{-2})	τ	τ ($n_{fas}=0$)	$(\tau_{JV})^{1/2}$	τ_{JV}
H_2	0.2	1.3	1.945	2.179	2.211	4.89
H_2	0.34	2.1	2.024	2.243	2.294	5.26
H_2	0.5	3.25	1.913	2.136	2.211	4.89
CO	0.18	0.21	2.730	2.871	2.876	8.27
CO	0.23	0.31	2.502	2.656	2.661	7.08
CO	0.32	0.49	2.311	2.475	2.484	6.17
CO	0.44	0.73	2.194	2.366	2.377	5.65

Fuel partial pressures (p.p.), anode saturation current densities (i_{as}), and τ_{JV} are from JV Table 2 [1].

Table 2
Tortuosities calculated for various ternary system diluent gases and partial pressures (p.p. in atm), and measured anode saturation current densities (i_{as}, A cm^{-2})

Diluent	p.p.	i_{as}	τ_{lin}	τ_{quad}	τ_{exact}	$(\tau_{JV})^{1/2}$	τ_{JV}
He	0.78	1.5	1.7159	1.7025	1.7025	2.3707	5.62
He	0.65	2.4	1.7295	1.7069	1.7068	2.3130	5.35
He	0.53	3.25	1.7371	1.7052	1.7051	2.2583	5.1
He	0.42	4	1.7634	1.7215	1.7214	2.2271	4.96
N_2	0.8	0.89	2.8705	2.8020	2.8029	2.7495	7.56
N_2	0.67	1.56	2.7149	2.6225	2.6240	2.6627	7.09
N_2	0.57	2.3	2.4401	2.3469	2.3484	2.4597	6.05
N_2	0.5	2.65	2.4467	2.3433	2.3450	2.4860	6.18
CO_2	0.81	0.7	3.4465	3.3183	3.3225	3.0000	9
CO_2	0.68	1.43	2.9452	2.8038	2.8094	2.6833	7.2
CO_2	0.6	1.88	2.8036	2.6560	2.6622	2.6153	6.84
CO_2	0.5	2.4	2.7221	2.5663	2.5730	2.6019	6.77

The first three and last columns are from JV [1].

A key parameter in determining the pressure gradient is the tortuosity τ, which is the ratio of the typical diffusion path length to the electrode thickness. Measurement of its value is needed for determining the quality of the anode pore configuration. Also, τ is a necessary parameter in any model for $V(i)$, and conversely we will show how our model for $V(i)$ provides a more accurate determination of τ.

The paper begins with a description of the Jiang–Virkar [1] experiment to which our analysis is applied. This is followed by a discussion of the Stefan–Maxwell equation including both Knudsen (molecule collisions with pore walls) and binary collision effects. Then the theory and results for binary and ternary anode gas mixtures are presented, followed by conclusions and recommendations.

2. Description of Jiang–Virkar experiment

Jiang and Virkar [1] performed a series of careful experiments on flow of various gas mixtures in the anode of an SOFC. This paper will be referred to as JV. JV studied binary system anode-side gas mixtures H_2/H_2O and CO/CO_2, and ternary systems with incoming H_2 fuel diluted with He, N_2, or CO_2. In all cases, the total metered inflow rate of the two gases was held at 140 mL min^{-1}, corresponding to 6.286×10^{19} molec s^{-1} as explained below. The "ternary" systems are called ternary because H_2O (steam) "exhaust" is produced at the anode–electrolyte interface and mixes with the hydrogen and diluent gas. We compare their calculations of tortuosity τ with values found from our analysis. We use the definition of tortuosity as the average actual path length traversed through the anode by a fuel or exhaust molecule, divided by the anode thickness. There are other definitions in the literature; in fact, the term "tortuosity" has a "tortuous" history [2]. In particular, JV and some others define tortuosity as what we and some others [2] call "tortuosity factor." The low range of τ values we obtain, from 1.7 to 3.3, is in accord with the 2.5–3 range found by Williford et al. [3] who criticized reports of "anomalously high" tortuosities in the 6–17 range.

In the JV experiments, the cathode-side gas was air. Both sides must have been at 1 atm sea level in order to reproduce their results, even though their laboratory is at the University of Utah, well above sea level. The partial pressures in atmospheres for the various metered input gases are given in our Tables 1 and 2 and Figs. 2 and 3. The temperature T was 800 °C = 1073 K for all their experiments. Their SOFC consisted of five layers, as shown in Fig. 1, and constructed of the materials listed below.

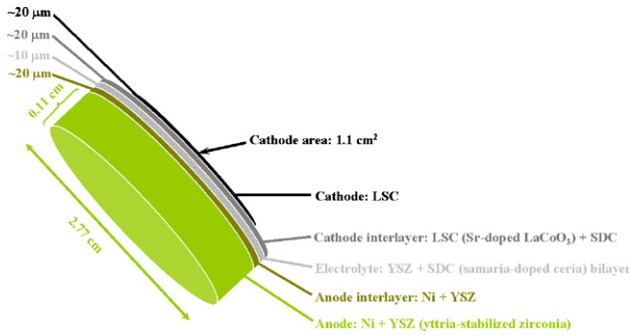|	
Anode	Ni + YSZ (yttria-stabilized zirconia)
Anode interlayer	Ni + YSZ
Electrolyte	YSZ + SDC (samaria-doped ceria) bilayer
Cathode interlayer	LSC (Sr-doped LaCoO$_3$) + SDC
Cathode	LSC

Fig. 1. Drawing of SOFC employed by Jiang and Virkar [1].

The anode thickness $w = 0.11\,cm$, and its porosity $\phi = 0.54$. Their estimated pore radius from SEM micrographs was $\sim 0.5\,\mu m$.

3. Dusty-gas model for gas flow in pores

The dusty-gas model consists of the Stefan–Maxwell equation including the Knudsen term. In molar units it is [1]

$$\frac{N_i}{D_{Ki}} + \sum_{j \neq i} \frac{X_j N_i - X_i N_j}{D_{ij}} = -\frac{(1/RT)\partial(PX_i)}{\partial x}, \tag{1}$$

where N_i and N_j are molar fluxes of components i and j ($mol\,cm^{-2}\,s^{-1}$), respectively, D_{Ki} and D_{ij} are the Knudsen diffusion coefficient for component i and the binary diffusion coefficient for components i and j, respectively, X_i and X_j are the fractional molar concentrations of components i and j, P is the total pressure, R is the gas constant, and T is the absolute temperature. We emphasize that x is the coordinate along a typical diffusion path, not across the anode, so the total diffusion path length is τw, the product of the tortuosity and the anode thickness. Note that this analysis ignores laminar flow (permeation flux) effects [4] which are considered unimportant in small pores.

Note further that Eq. (1) is modified from Eq. (9) of the JV paper in that P is outside the derivative in their paper. That is correct only in the approximation that P is independent of position. The total pressure of the incoming gases and the gases in the plenums is one atmosphere, denoted as P_1, but the total pressure P in the anode and cathode pores will be a function of position in the pore. We will show that P varies across the anode by amounts of order 10%.

The Knudsen diffusion coefficient only considers collisions with the wall, and from the kinetic theory of gases is

$$D_{K,i} = \frac{2}{3}\left(\frac{8RT}{\pi M_i}\right)^{1/2} \bar{r}, \tag{2}$$

where $\bar{r}$ is the mean pore radius (0.5 μm) and M_i is the molar mass. At 1073 K the D_{Ki} values for this pore radius are 11.3 and $3.00\,cm^2\,s^{-1}$ for H_2 and CO, respectively. To convert Eq. (2) to molecular units, we replace R/M_i by k/m_i, where k is Boltzmann's constant, $1.38 \times 10^{-23}\,J\,K^{-1}$ and m_i is molecular mass. We convert to molecular units to make some equations simpler.

The binary diffusion coefficients D_{ij} for various gas–molecule pairs at three temperatures are tabulated in JV Table 1. The coefficients for the two 2-species cases, H_2/H_2O and CO/CO_2, have D_{ij1} values of 7.704 and $1.408\,cm^2\,s^{-1}$, respectively at 1073 K. The subscript 1 indicates that the values are for 1 atm total pressure.

To convert Eq. (1) to molecular units, several steps are necessary. The X_i are dimensionless mole or molecular fractions of the total gas concentration. The N_i are converted to J_i molecules per unit area and time by multiplying by Avogadro's number N_A. The gas constant R has moles in the denominator, so putting N_A in the numerator changes R to k. But $P = nkT$, where n is the total number of gas molecules per unit volume, so the kT factors cancel. Since $nX_i = n_i$, the right side of Eq. (1) is simply $-\partial n_i / \partial x$. D_{ij} has the total concentration n in its denominator, but since D_{ij} itself is in the denominator in Eq. (1), n appears in the numerator in that term, and n multiplied by X_i or X_j changes them to n_i or n_j. Thus, Eq. (1) converts to

$$\frac{J_i}{D_{Ki}} + \frac{(J_i n_j - J_j n_i)kT}{D_{ij1} P_1} = -\frac{\partial n_i}{\partial x}. \tag{3}$$

Here, D_{ij1} is the binary diffusion coefficient at $P_1 \equiv 1$ atm, and the nkT-type terms in the numerator divided by P_1 convert D_{ij1} to D_{ij} at the actual total pressure at any position x along the anode pore.

The variable x is distance along the pore, so the total length L of the pore is $L = \tau w$, where τ is the anode pore tortuosity and w is the 0.11 cm thickness of the anode.

4. Calculation for binary gas input

For the two binary gas systems H_2/H_2O and CO/CO_2, if subscript f is for the fuel gas and e is for the exhaust gas, $J_e = -J_f$ in Eq. (3). Here, $J_f = i\tau/\phi q$, where i is the current density ($A\,cm^{-2} = C\,cm^{-2}s^{-1}$) in the solid electrolyte and q is the charge ($3.2 \times 10^{-19}\,C\,molecule^{-1}$) carried per gas molecule annihilated/created in the reaction at the anode/electrolyte interface.

The τ/ϕ factor is an enhancement factor by which the flow density J_i is enhanced compared to its value if the anode were completely porous ($\phi = \tau = 1$). To derive this result, note that this enhancement factor for an anode of area S with N_{pa} pores each of cross-sectional area A_x is $S/N_{pa}A_x$. The porosity ϕ is the total pore volume $N_{pa}A_x\tau w$ divided by the anode volume Sw, so $\phi = N_{pa}A_x\tau/S$. By rearranging this equation we find that the enhancement factor $S/N_{pa}A_x$ is τ/ϕ.

Eq. (3) for the fuel gas can now be written, after setting $n_e + n_f = n$, as

$$\frac{\partial n_f}{\partial x} = -\left(\frac{i\tau}{\phi q}\right)\left(\frac{1}{D_{Kf}} + \frac{nkT}{D_{ef1}P_1}\right) \equiv -c_3\tau - c_4 n\tau, \tag{4}$$

where c_3 and c_4 are positive constants, and subscript f refers to the fuel gas (H_2 or CO) in the binary gas system. The corresponding equation for the exhaust gas, after defining $(m_e/m_f)^{1/2} \equiv 2h + 1$, is

$$\frac{\partial n_e}{\partial x} = (2h + 1)c_3\tau + c_4 n\tau. \tag{5}$$

Adding Eqs. (4) and (5) yields the equation for n and its solution,

$$\frac{\partial n}{\partial x} = 2hc_3\tau, \quad n = n_1 + 2hc_3\tau x. \tag{6}$$

From the ideal gas law, $P = nkT$, we see that the total pressure P increases linearly with x, in going through the anode from the plenum to the solid electrolyte.

Now that $n(x)$ is known, we can solve Eq. (4) for n_f.

$$\frac{\partial n_f}{\partial x} = -c_3\tau - c_4(n_1 + 2hc_3\tau x)\tau, \quad n_f = n_{fp} - (c_3 + c_4 n_1)\tau x - hc_3 c_4 \tau^2 x^2, \tag{7}$$

where n_{fp} is the concentration of fuel gas in the plenum, which will be found below. We see that n_f, and thus $n_e = n - n_f$, vary both linearly and quadratically with x.

If the cell current density is limited by anode saturation, designated as i_{as} by JV, then i becomes i_{as} in Eq. (4) and in the constants c_3 and c_4, which are designated c_{3as} and c_{4as} for the anode saturation condition. In previous works [1,5] the approximation was made that in this limit the fuel concentration n_f reaches zero at the anode–electrolyte interface where $x = \tau w$. This approximation obviously cannot be exactly correct, because i_{as} cannot be positive for zero fuel concentration, whereas the measured i_{as} is positive.

To avoid making this unphysical approximation, we use results from our recent analysis of SOFC voltage V as a function of current density i [8]. This relation is

$$V(i) = \frac{U}{q} - \frac{kT}{q}\ln\left[\frac{(b + i)(d + i)^{1/2}}{(a - i)(c - i)^{1/2}}\right] - V_{ohm}. \tag{8}$$

Here, U is the enthalpy for the gas-state reaction $H_2 + 1/2 O_2 \rightarrow H_2O$ or $CO + 1/2 O_2 \rightarrow CO_2$ at 800 °C and 1 atm for all constituents, q is the reaction charge transfer of 2e, k is Boltzmann's constant, T is absolute temperature, and V_{ohm} is the ohmic polarization. Unlike other $V(i)$ expressions in the literature (see [8]), Eq. (8) puts all four reaction attempt current densities a, b, c, d on the same footing. The forward and reverse anode attempt current densities are a and b, while the forward and reverse cathode attempt current densities are c and d. These reaction attempt current densities are multiplied by reaction success probabilities which are functions of k, T, q, i, and anode and cathode contributions to U, to find anode and cathode contributions to V in Eq. (8). Eq. (15) shows the form of a, and the other incoming gas reaction attempt current densities b and c have similar forms. Other authors (see [8]) have factors in the ln argument corresponding more or less to ours that involve a, b, and c, though these factors involve partial pressures whereas ours involve concentrations and molecular velocities. No other authors to our knowledge explicitly show a factor corresponding to our $(d + i)^{1/2}$ factor, where d is the attempt current density corresponding to oxygen ions from the electrolyte combining to form O_2 gas. This factor is much larger than the other three factors in the ln argument, and reduces the open-circuit emf considerably below the value of 1.214 V for U/q. Other authors instead implicitly incorporate the $-(kT/q)\ln[(d + i)^{1/2}]$ term as an entropy term as part of the reaction Gibbs energy G, and present the known G in G/q in place of our U/q as the first term in $V(i)$. Fortunately, our d expression [8] based on a molecular model for that reaction attempt rate gives approximately the correct open-circuit emf and thus provides a check on that reaction model.

The terminal voltage V is often expressed as a sum of terms

$$V = V_0 - V_{act} - V_{conc} - V_{ohm}, \tag{9}$$

and each term can be found separately as shown below. The open-circuit emf V_0, from Eq. (8) with $i = V_{ohm} = 0$, and with a, b, c, d set at their open-circuit values a_0, b_0, c_0, d_0, is

$$V_0 = \frac{U}{q} - \frac{kT}{q} \ln \frac{b_0 d_0^{1/2}}{a_0 c_0^{1/2}}. \tag{10}$$

The activation polarization from Eq. (9) is given by $V_{act} = V_0 - V - V_{conc} - V_{ohm}$. It signifies the voltage drop required to provide a given i for fixed gas concentrations at the electrode interfaces with the electrolyte. If we set $a = a_0$, etc. in Eq. (8) we eliminate V_{conc} because the gas concentrations at the electrode interfaces with the electrolyte depend only on a, b, and c. If we also eliminate V_{ohm} in Eq. (8), then Eq. (8) becomes

$$V_0 - V_{act} = \frac{U}{q} - \frac{kT}{q} \ln \frac{(b_0 + i)(d_0 + i)^{1/2}}{(a_0 - i)(c_0 - i)^{1/2}}, \tag{11}$$

so V_{act} is found by subtracting the Eq. (11) from the Eq. (10) expression,

$$V_{act} = \frac{kT}{q} \ln \frac{a_0 c_0^{1/2} (b_0 + i)(d_0 + i)^{1/2}}{b_0 d_0^{1/2} (a_0 - i)(c_0 - i)^{1/2}}. \tag{12}$$

Inserting expressions from Eqs. (8) and (12) into Eq. (9), we obtain

$$V_{conc} = \frac{kT}{q} \ln \frac{(a_0 - i)(b + i)(c_0 - i)^{1/2}(d + i)^{1/2}}{(a - i)(b_0 + i)(c - i)^{1/2}(d_0 + i)^{1/2}}. \tag{13}$$

The meaning of V_{conc} is the additional voltage drop required because increasing i causes changes in gas concentrations at the electrode interfaces with the electrolyte. An important fact, generally not mentioned, is that there are two contributions to V_{conc}. The one that usually comes to mind is the change with i of gas concentrations as one goes across the electrodes. The other contribution is the dependence on i of gas partial pressures and concentrations in the plenums which occurs even if there is no concentration change across the electrodes and the feed gas flow rates remain fixed. Both contributions are discussed below. Both V_{act} and V_{conc} take on the sign of i. The sum of V_{act} and V_{conc} is

$$V_{act} + V_{conc} = \frac{kT}{q} \ln \frac{a_0 c_0^{1/2} (b + i)(d + i)^{1/2}}{b_0 d_0^{1/2} (a - i)(c - i)^{1/2}}. \tag{14}$$

The saturation current density i_{as} is defined as the current density at which V drops to zero, but from both experiment and our $V(i)$ model [8] the voltage drops extremely rapidly toward $-\infty$ as i goes through i_{as}. Accordingly, to a very good approximation, i_{as} is the current density at which (an applied) V approaches $-\infty$. From Eq. (8), this occurs for $i_{as} = a$.

Our model [8] gives a relation between a and n_f, allowing us to find the n_f value n_{fas} attained at the anode saturation condition where $a = i_{as}$. This relation is

$$a = \frac{1}{2} n_f \left(\frac{kT}{m_f} \right)^{1/2} q(1 - v_a) f_a, \tag{15}$$

where m_f is the fuel molecule mass, $(kT/m_f)^{1/2}$ is the fuel molecule average velocity component (through the anode pore) directed toward the triple phase boundary (TPB), $1 - v_a$ is the probability that an O^{2-} site at the anode TPB will be occupied (not vacant) so the fuel oxidation reaction can occur, and f_a is the probability that the fuel molecule strikes the electrolyte at an anode TPB. The Eq. (15) relation is model-dependent, but it seems that in any model there will be a linear or nearly linear relation between a and n_f.

Going back now to Eq. (7), we can no longer set $n_f(x = L = \tau w) = 0$, but instead we designate it as n_{fas}. We then obtain a quadratic equation for τ^2, valid for the anode saturation condition

$$hc_{3as} c_{4as} w^2 \tau^4 + (c_{3as} + c_{4as} n_1) w \tau^2 - n_{fpas} + n_{fas} \equiv A\tau^4 + B\tau^2 + C = 0. \tag{16}$$

All constants in Eq. (16) except C are positive, so in the solution

$$\tau^2 = \frac{-B \pm (B^2 - 4AC)^{1/2}}{2A}, \tag{17}$$

we must choose the $+$ sign so that τ^2 will be positive.

All constants in Eq. (16) have been defined except for the boundary conditions n_1 and n_{fpas} for the total and fuel gas concentrations, respectively in the plenum at the outer anode surface, and n_{fas} for the fuel gas concentration at the anode–electrolyte interface. For the JV experiments, $n_1 = P_1/kT$ where $P_1 = 1$ atm $= 1.015 \times 10^5$ N m^{-2} and $T = 1073$ K, so $n_1 = 6.855 \times 10^{18}$ cm^{-3}.

To find n_{fpas} we consider the total flow in and out of the anode plenum. From the discussion in JV p. A943 it appears that for all the binary and ternary systems displayed in JV Table 2, the metered gas inflow rate of 140 mL min^{-1} is for two gases, so that in the ternary systems the third gas is H_2O generated at the anode–electrolyte interface. This total metered inflow rate of 140 mL min^{-1} at a temperature of $T_{in} = 273$ K and at 1 sea level atmosphere is, from the ideal gas law,

$$P_1 \frac{dV_{in}}{dt} = kT_{in} \frac{dN_{in}}{dt}, \quad \text{so} \quad \frac{dN_{in}}{dt} \equiv j_1 = 6.286 \times 10^{19} \text{ molec s}^{-1}. \tag{18}$$

JV did not specify the temperature at the metered inflow, but $T_{in} = 273$ K fits their results best, based on solving for m_T from Eq. (32) of JV using $D_{H2,eff}$, i_{as}, and p_{H2} from JV Table 2 for the three H_2/H_2O runs. The metered inflow of each gas constituent is found by multiplying the total metered inflow rate by the partial pressure fraction given or implied in JV Table 2. For instance, the first entry is $p_f = 0.2$ for H_2, so $p_e = 0.8$ for H_2O. Though these Table 2 entries are in atmospheres, in this analysis we define these ps as dimensionless partial pressure fractions. Then the respective metered inflow rates are: $j_{fm} = p_f j_1 = 1.257 \times 10^{19}$ s^{-1} and $j_{em} = p_e j_1 = 5.029 \times 10^{19}$ s^{-1}. We assume here that the p values in JV Table 2 are really p^o values, where p^o is the partial pressure of the metered incoming fuel or diluent as defined below Eq. (26) of JV.

To find the net inflow of each gas into the plenum, we must also consider the fuel gas outflow into the anode, and the exhaust gas inflow from the anode. These flows are equal and opposite, and are given by $j_e = -j_f = iS/q$, where S is the active area of 1.1 cm^2 and $q = 3.2 \times 10^{-19}$ C. Using again the first entry in JV Table 2, $i_{as} = 1.3$ A cm^{-2}, we find H_2 outflow $j_{fas} = -4.469 \times 10^{18}$ molec s^{-1} and H_2O inflow $j_{eas} = +4.469 \times 10^{18}$ molec s^{-1}. Comparison of the H_2 outflow with the metered H_2 inflow gives a fuel utilization $-j_{fas}/j_{fm}$ of 35.5% for this example.

From the numbers in the previous two paragraphs, the net H_2 inflow into the plenum is $j_{fnet} = j_{fm} + j_{fas} = 8.104 \times 10^{18}$ molec s^{-1} and the net H_2O inflow is $j_{enet} = j_{em} + j_{eas} = 5.476 \times 10^{19}$ molec s^{-1}, for a total net inflow to the plenum of $j_1 = 6.286 \times 10^{19}$ s^{-1}. The outflow from the plenum to the atmosphere must contain the corresponding fractions, $-j_{fnet}/j_1 = 0.1289$ for H_2 and $j_{enet}/j_1 = 0.8711$ for H_2O, on a molecular basis. These values are considerably different from the corresponding metered inflow fractions, $p_f = 0.2$ and $p_e = 0.8$. To summarize the analytic expression for j_{fnet} and j_{enet},

$$j_{fnet} = p_f j_1 - \frac{iS}{q}; \quad j_{enet} = (1 - p_f)j_1 + \frac{iS}{q}. \tag{19}$$

One must consider whether the mole fractions in the plenum are the same as the mole fractions in the outflow. For openings small compared to the mean free path, this is not the case, because the outflow rate per molecule in the plenum is inversely proportional to the square root of the molecular mass [6]. However, it seems probable that the outflow arrangement provided by JV result in the mole fractions in the plenum being essentially the same as in the outflow. We assume that the gases in the plenum are well mixed and have the same mole fractions everywhere. Accordingly, in the plenum the fuel and exhaust concentrations under anode saturation conditions are

$$n_{fpas} = \left(\frac{j_{fas}}{j_1} \right) n_1 = \left(p_f - \frac{i_{as}}{i_1} \right) n_1; \quad j_{epas} = \left(\frac{j_{eas}}{j_1} \right) n_1 = \left(1 - p_f + \frac{i_{as}}{i_1} \right) n_1, \tag{20}$$

where p_f and i_{as} are values taken from JV Table 2, and $i_1 = j_1 q/S = 18.29$ A cm^{-2}.

The remaining parameter to determine is n_{fas}, the fuel gas concentration at the anode–electrolyte interface under the anode saturation condition. From Eq. (15), n_f remains proportional to a as i changes, because we assume the other parameters are independent of i. For open-circuit ($i = 0$) conditions, n_f at the interface equals n_{f0} at the plenum, which from Eq. (20) will be $p_f n_1$ for open-circuit. This known value for open-circuit n_f inserted into Eq. (15) provides a known value $a_0 = p_f a_{01}$ for the open-circuit value of a, where a_{01} is the open-circuit value for $p_f = 1$. For the anode saturation condition, $a = i_{as}$, and because n_f is proportional to a, $n_{fas} = n_{f0} a_{as}/a_0 = p_f n_1 i_{as}/p_f a_{01} = n_1 i_{as}/a_{01}$. Inserting this n_{fas} value and the above n_{fpas} value into Eq. (16) yields the following equation for τ^2 in terms of known parameters

$$hc_{3as}c_{4as}w^2\tau^4 + (c_{3as} + c_{4as}n_1)w\tau^2 - \left(p_f - \frac{i_{as}}{i_1} \right) n_1 + n_1 \frac{i_{as}}{a_{01}} \equiv A\tau^4 + B\tau^2 + C = 0. \tag{21}$$

In our previous analysis [5] the $n_1 i_{as}/a_{01}$ term was missing.

5. Results for binary gas input

We are now in a position to use Eqs. (21) and (17) to find τ

$$\tau = \left\{ \frac{-B + (B^2 - 4AC)^{1/2}}{2A} \right\}^{1/2}. \tag{22}$$
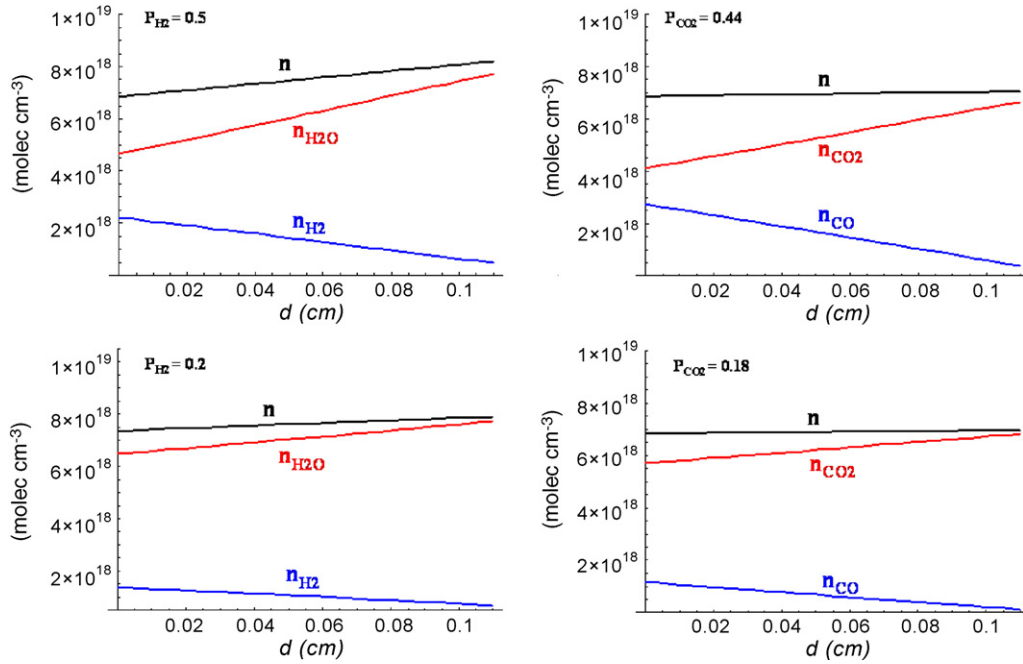
Fig. 2. Plots of gas concentrations *vs.* position in anode for some binary gas inputs under anode limiting current conditions.

We begin by summarizing the constants that appear directly or indirectly in Eq. (16), and that do not change from run to run. They are provided here to aid the reader who may want to check the numerical results of this study that appear in Table 1 and Fig. 2. The meanings of the symbols are explained above where the symbols first appear.

$$\phi = 0.54, \qquad q = 3.2 \times 10^{-19}\,\text{C}, \qquad k = 1.38 \times 10^{-23}\,\text{J K}^{-1}, \qquad T = 1073\,\text{K}, \qquad P_1 = 1.015 \times 10^5\,\text{N m}^{-2},$$

$$w = 0.11\,\text{cm}, \qquad n_1 = 6.855 \times 10^{18}\,\text{cm}^{-3}, \qquad i_1 = 18.29\,\text{A cm}^{-2}, \qquad a_{01} = 48.4\,\text{A cm}^{-2},$$

$$D_{\text{Kf}} = 11.3\,\text{cm}^2\,\text{s}^{-1}(\text{H}_2);\ 3.00\,\text{cm}^2\,\text{s}^{-1}(\text{CO}),$$

$$D_{\text{ef1}} = 7.704\,\text{cm}^2\,\text{s}^{-1}\ (\text{H}_2, \text{H}_2\text{O}) = 1.408\,\text{cm}^2\,\text{s}^{-1}(\text{CO}, \text{CO}_2),$$

$$\frac{c_{3as}}{i_{as}} = \frac{1}{\phi q D_{\text{Kf}}} = 5.121 \times 10^{17}\,\text{s C}^{-1}\,\text{cm}^{-2}(\text{H}_2) = 1.929 \times 10^{18}\,\text{s C}^{-1}\,\text{cm}^{-2}(\text{CO}),$$

$$\frac{c_{4as}}{i_{as}} = \frac{kT}{\phi q D_{\text{ef1}} P_1} = 0.1096\,\text{cm s C}^{-1}(\text{H}_2) = 0.5994\,\text{cm s C}^{-1}(\text{CO}),$$ (23)

$$h = \frac{(m_e/m_f)^{1/2} - 1}{2} = 1(\text{H}_2), = 0.1268(\text{CO}),$$

$$n_{\text{fpas}} = -C = \left(p_f - \frac{i_{as}}{i_1} - \frac{i_{as}}{a_{01}}\right) n_1, \qquad A = h c_{3as} c_{4as} w^2, \qquad B = (c_{3as} + c_{4as} n_1) w.$$

We carry out a sample calculation for the first entry in JV Table 2, for the H_2/H_2O binary system, for which $p_f = 0.2$ and $i_{as} = 1.3\,\text{A cm}^{-2}$. Various parameters used in this calculation and whose meanings are explained above are

$$a_{01} = 48.4\,\text{A cm}^{-2}, \qquad a_0 = p_f a_{01} = 9.68\,\text{A cm}^{-2}\ \text{from our}\ V(i)\ \text{analysis [8]}$$

$$c_{3as} = 6.657 \times 10^{17}\,\text{cm}^{-4}, \qquad c_{4as} = 0.1425\,\text{cm}^{-1}, \qquad A = 1.148 \times 10^{15}\,\text{cm}^{-3}, \qquad B = 1.807 \times 10^{17}\,\text{cm}^{-3},$$

$$C = -6.996 \times 10^{17}\,\text{cm}^{-3}\ (\text{Ref. [5] value} - 8.836 \times 10^{17}\,\text{cm}^{-3}),$$ (24)

$$(B^2 - 4AC)^{1/2} = 1.894 \times 10^{17}\,\text{cm}^{-3}\ (\text{Ref. [5] value}\ 1.916 \times 10^{17}\,\text{cm}^{-3}),$$

$$\tau = 1.944\,(\text{Ref. [5] value}\ 2.179), \qquad \text{JV}\ \tau^{1/2} = 2.211, \qquad \text{JV}\ \tau = 4.89.$$

These results and those for the other two H_2/H_2O data sets from JV appear in Table 1.

It is highly encouraging that our τ values agree well with each other, and especially that their small magnitudes seem very reasonable for the high-porosity ($\phi = 0.54$) anode that JV investigated. They agree fairly well also with the JV results in the $(\tau_{JV})^{1/2}$ column, where it is taken into account that what JV call tortuosity in the τ_{JV} column is the tortuosity factor [2] whose square root is what we and others call tortuosity. To calculate the τ values for the four data sets from JV for the CO/CO_2 binary system, the above

analysis is unchanged except that subscripts f and e refer to CO and CO_2, respectively. The tortuosity results are given in Table 1 below.

We see in Table 1 that our previous [5] analysis results [$\tau(n_{\text{fas}}=0)$] which range from about 2.1 to 2.9 agree better than our present results [τ] which range from about 1.9 to 2.7, with the Jiang–Virkar [1] results [$(\tau_{\text{JV}})^{1/2}$] which range from about 2.2 to 2.9. This occurs because our previous analysis differed from theirs only by our allowing total pressure to vary along the pore, and by consequences of that variation. Our present analysis also takes into account that the fuel concentration is nonzero under anode saturation conditions, unlike our previous analysis and that of Jiang and Virkar. The result as seen in Table 1 is that our present tortuosity values are smaller than our previous values by roughly 10%. We consider that these lower values are more accurate, but it must be remembered that the previous analyses by JV and ourselves were independent of a model for $V(i)$. Our confidence on the approximate validity of this 10% reduction is based on the accuracy with which our $V(i)$ model [8] fits the $V(i)$ curves of JV for the H_2/H_2O binary system.

Plots of gas concentrations *vs.* position in the anode appear in Fig. 2 for the lowest and highest H_2 and CO fuel concentrations in the anode plenum. The total concentration, and thus total pressure, has much stronger position dependence for H_2 than for CO fuel. This strong dependence of total pressure on position in the anode shows that the commonly made assumption of uniform total pressure across the anode is a serious approximation. The quadratic contribution to the position dependences for the various fuel and exhaust concentrations is barely visible.

6. Calculation for ternary gas input

The ternary systems consisted of incoming H_2 fuel diluted with He, N_2, or CO_2. They are ternary because H_2O (steam) "exhaust" is produced at the anode–electrolyte interface. We will compare the JV calculations of tortuosity τ with values found from our analysis.

In the preceding analysis of the binary systems, we used subscripts e and f for exhaust and fuel gases, respectively. For the ternary systems, we will use subscripts d for the He, N_2, or CO_2 diluent gases, e for the H_2O exhaust gas, and f for the H_2 fuel gas.

We note that for H_2 fuel and H_2O exhaust, in the Stefan–Maxwell equations the molar flow rates obey $N_d = 0$ and $N_e = -N_f$ and we denote N_f by N. Then Eq. (1) becomes

$$\frac{N}{D_{\text{Kf}}} + \frac{X_d N}{D_{\text{df}}} + \frac{(X_f + X_e)N}{D_{\text{ef}}} = -\frac{1}{RT}\frac{\mathrm{d}(PX_f)}{\mathrm{d}x},$$
$$-\frac{N}{D_{\text{Ke}}} - \frac{X_d N}{D_{\text{de}}} - \frac{(X_f + X_e)N}{D_{\text{ef}}} = -\frac{1}{RT}\frac{\mathrm{d}(PX_e)}{\mathrm{d}x},$$
$$-\frac{X_d N}{D_{\text{df}}} + \frac{X_d N}{D_{\text{de}}} = -\frac{1}{RT}\frac{\mathrm{d}(PX_d)}{\mathrm{d}x}. \tag{25}$$

The third equation, for the diluent gas, is absent for binary systems.

First we convert to molecular units by multiplying through by Avogadro's number. This converts N to J, which has units of molecules $\text{cm}^{-2}\,\text{s}^{-1}$, and converts R to k which is Boltzmann's constant. Thus $1/RT$ becomes $1/kT$. From the ideal gas law, $P = nkT$, so $(1/kT)\mathrm{d}(PX_f)/\mathrm{d}x = \mathrm{d}(nX_f)/\mathrm{d}x = \mathrm{d}n_f/\mathrm{d}x$, etc. These are the concentration gradients in cm^{-4}. Here n is the total gas concentration and n_f, etc. are the partial concentrations, in cm^{-3}.

We can then write Eq. (25) in terms of molecular units as

$$\frac{\mathrm{d}n_f}{\mathrm{d}x} = -\frac{J}{D_{\text{Kf}}} - \frac{J X_d}{D_{\text{df}}} - \frac{J(X_e + X_f)}{D_{\text{ef}}},$$
$$\frac{\mathrm{d}n_e}{\mathrm{d}x} = \frac{J}{D_{\text{Ke}}} + \frac{J X_d}{D_{\text{de}}} + \frac{J(X_e + X_f)}{D_{\text{ef}}},$$
$$\frac{\mathrm{d}n_d}{\mathrm{d}x} = \frac{J X_d}{D_{\text{df}}} - \frac{J X_d}{D_{\text{de}}}. \tag{26}$$

The quoted D_{ij} values in JV Table 1, which we call D_{ij1}, are based on 1 atmosphere pressure, which we label P_1. Accordingly, using the ideal gas law $P = nkT$, noting that P is in the denominator of D_{ij}, and letting n_1 be the total gas concentration at $T = 1073$ K,

$$\frac{1}{D_{ij}} = \frac{P}{P_1 D_{ij1}} = \frac{n}{n_1 D_{ij1}}. \tag{27}$$

Finally, we note that $X_i = n_i/n$, etc., so we can rewrite Eq. (26) as

$$\frac{dn_f}{dx} = -\frac{J}{D_{Kf}} - \frac{J}{n_1}\left[\frac{n_d}{D_{df1}} + \frac{(n_e + n_f)}{D_{ef1}}\right],$$

$$\frac{dn_e}{dx} = \frac{J}{D_{Ke}} + \frac{J}{n_1}\left[\frac{n_d}{D_{de1}} + \frac{n_e + n_f}{D_{ef1}}\right], \tag{28}$$

$$\frac{dn_d}{dx} = -\left(\frac{Jn_d}{n_1}\right)\left(\frac{1}{D_{de1}} - \frac{1}{D_{df1}}\right).$$

Adding these three equations and noting that $n_d + n_e + n_f = n$ yields an equation for n and its solution,

$$\frac{dn}{dx} = J\left(\frac{1}{D_{Ke}} - \frac{1}{D_{Kf}}\right), \quad n = n_1(1 + c_5 x); \quad c_5 \equiv \left(\frac{J}{n_1}\right)\left(\frac{1}{D_{Ke}} - \frac{1}{D_{Kf}}\right) > 0. \tag{29}$$

In solving the dn_d/dx equation in Eq. (28) for n_d, we get

$$n_d = n_{dp}\exp(c_7 x); \quad c_7 \equiv -\left(\frac{J}{n_1}\right)\left(\frac{1}{D_{de1}} - \frac{1}{D_{df1}}\right) < 0. \tag{30}$$

Jiang and Virkar [1] pointed out this exponential nature of the diluent gas concentration dependence on position, but omitted using this dependence to simplify their calculations. This non-vanishing concentration dependence on x may seem surprising because the diluent gas has no net flow in the pores. It occurs because of the unlike masses of the fuel and exhaust molecules that the diluent molecules collide with. The >0 and <0 relations occur in Eqs. (29) and (30), respectively because for the systems studied, the exhaust molecule is more massive than the fuel molecule and the inverse Knudsen and binary diffusion coefficients increase with molecular mass. Accordingly, Eq. (29) tells us that total gas concentration increases linearly with x, whereas Eq. (30) tells us that diluent gas concentration decreases exponentially with x.

Because n_1 and n_{dp} are known as explained below, we can solve for n_e in terms of n_f

$$n_e = n - n_d - n_f = n_1(1 + c_5 x) - n_{dp}\exp(c_7 x) - n_f. \tag{31}$$

Then the dn_f/dx equation in Eq. (28) becomes

$$\frac{dn_f}{dx} = -J\left[\frac{1}{D_{Kf}} + \frac{1 + c_5 x}{D_{ef1}}\right] + \frac{Jn_{dp}}{n_1}\left(\frac{1}{D_{ef1}} - \frac{1}{D_{df1}}\right)\exp(c_7 x). \tag{32}$$

The solution to this equation can be written as

$$n_f = n_{fp} + n_{dp}g[1 - \exp(c_7 x)] - \left(\frac{J}{D_{Kf}}\right)x - \frac{J}{D_{ef1}}\left(x + \frac{1}{2}c_5 x^2\right); \quad g \equiv \frac{(1/D_{ef1}) - (1/D_{df1})}{(1/D_{de1}) - (1/D_{df1})}. \tag{33}$$

Eq. (33) is especially useful under the condition of anode saturation. Under that condition we previously [5] set n_f equal to zero at the electrolyte interface, where $x = L = \tau w$, but as explained in the binary system analysis, we now set $n_f = n_{fas}$, its nonzero value for the current density value i_{as} for which the output voltage V drops rapidly through zero on its way to $-\infty$.

We also need expressions for n_{dp} and n_{fp} under the anode saturation condition. To find these, we note that under this condition the net flow rates in molec s^{-1} into the anode plenum are

$$j_d = j_1 p_d, \quad j_e = \frac{i_{as}S}{q}, \quad j_f = j_1(1 - p_d) - \frac{i_{as}S}{q}. \tag{34}$$

The total of these flow rates into the plenum is simply j_1. Here, i_{as} is the anode saturation current density as given in JV Table 2, S is the electrode area of 1.1 cm^2, q is the charge of 3.2×10^{-19} C per gas molecule created or destroyed at the anode/electrolyte interface, and p_d is the fractional partial pressure of the diluent gas, given in JV Table 2 as p_{He}, p_{N_2}, or p_{CO_2}. Note that the superscript o used in Eq. (26) of JV for metered incoming gas is missing in JV Table 2. One finds the total incoming molecular flow rate j_1 from the ideal gas law, $P_1 V_{in} = N_{in}kT_{in}$, using

$$j_1 \equiv \frac{dN_{in}}{dt} = \frac{P_1}{kT_{in}}\frac{dV_{in}}{dt}, \tag{35}$$

using dV_{in}/dt as 140 cm^3 min^{-1} as stated by JV for all experiments. In Eq. (35) we use $T_{in} = 273$ K to best fit the results of JV using their calculational method, so $j_1 = 6.286 \times 10^{19}$ molec s^{-1}.

As discussed for the binary systems, the net flow rates into the plenum equal the flow rates out of the plenum exit orifice, and these exit orifice flow rates are proportional to the gas concentrations in the plenum, so

$$n_{dp} = \frac{j_d}{j_1} n_1 = p_d n_1, \qquad n_{fp} = \frac{j_f}{j_1} n_1 = \left(1 - p_d - \frac{i_{as} S}{q j_1}\right) n_1 \equiv \left(1 - p_d - \frac{i_{as}}{i_1}\right) n_1; \quad i_1 \equiv \frac{q j_1}{S}. \tag{36}$$

Finally, we find J under the anode saturation condition, as discussed for the binary systems

$$J_{as} = \frac{i_{as} \tau}{\phi q}. \tag{37}$$

We can now write Eq. (33) under the anode saturation condition and evaluated at $x = \tau w$. From Eqs. (29), (30), and (37), we see that c_5 and c_7 depend linearly on τ. Accordingly, we must use the τ-independent factors $c_6 = c_5 w / \tau$ and $c_8 = c_7 w / \tau$ to display the true τ dependence.

$$n_{fas}(x = L = \tau w) = \left(1 - p_d - \frac{i_{as}}{i_1}\right) n_1 + p_d n_1 g [1 - \exp(c_8 \tau^2)] - \frac{i_{as} w}{\phi q D_{Kf}} \tau^2 - \frac{i_{as} w}{\phi q D_{ef1}} \left(\tau^2 + \frac{1}{2} c_6 \tau^4\right). \tag{38}$$

This is a transcendental equation for τ^2 that can be solved numerically. Written out explicitly by substituting for c_5, c_7, and g from Eqs. (23), (24), and (27), respectively, it appears as

$$\left(1 - p_d - \frac{i_{as}}{i_1} - \frac{i_{as}}{a_{01}}\right) n_1 - \frac{i_{as} w}{\phi q D_{Kf}} \tau^2 - \frac{i_{as} w}{\phi q D_{ef1}} \left[\tau^2 + \frac{1}{2} \left(\frac{i_{as} w}{\phi q n_1}\right) \left(\frac{1}{D_{Ke}} - \frac{1}{D_{Kf}}\right) \tau^4\right]$$

$$+ p_d n_1 \left[\frac{(1/D_{ef1}) - (1/D_{df1})}{(1/D_{de1}) - (1/D_{df1})}\right] \left\{1 - \exp\left[\frac{-i_{as} w}{\phi q n_1} \left(\frac{1}{D_{de1}} - \frac{1}{D_{df1}}\right) \tau^2\right]\right\} = 0. \tag{39}$$

In Eq. (39), we use $n_{fas} = n_1 i_{as} / a_{01}$ as we did for the binary system.

7. Results for ternary gas input

The relations in the equations below are useful in solving Eq. (39) numerically for the tortuosity τ values presented in Table 2 and Fig. 3. The D_{de1} values below are calculated from Eq. (2.22) and Tables 2.2 and 2.3 of *Mass Transfer* [7]. The constants that remain the same from one run to the next are
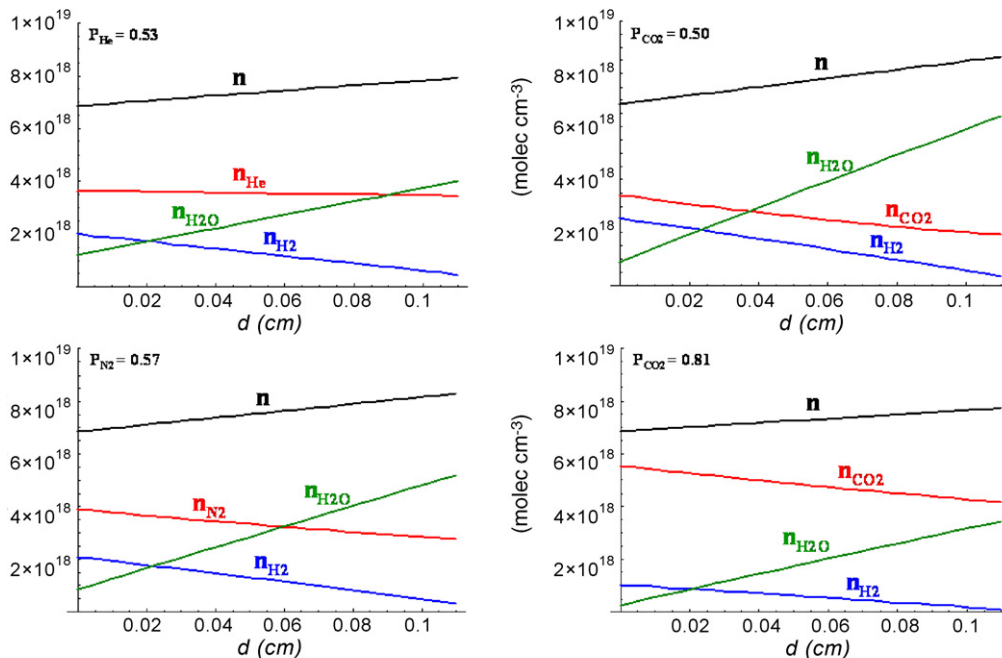

Fig. 3. Plots of gas concentrations *vs.* position in anode for some ternary gas inputs under anode limiting current conditions.

$$D_{Ke} = 3.767, \qquad D_{Kf} = 11.3, \qquad D_{ef1} = 7.704 \, \text{cm}^2 \, \text{s}^{-1},$$

$$D_{de1} = 7.462, \qquad D_{df1} = 13.29 \quad \text{for d} = \text{He},$$

$$D_{de1} = 2.21, \qquad D_{df1} = 6.303 \quad \text{for d} = \text{N}_2,$$

$$D_{de1} = 1.73, \qquad D_{df1} = 5.56 \quad \text{for d} = \text{CO}_2,$$

$$\frac{1}{D_{de1}} - \frac{1}{D_{df1}} = 0.05877 \, \text{s} \, \text{cm}^{-2} \quad \text{for d} = \text{He},$$

$$\frac{1}{D_{de1}} - \frac{1}{D_{df1}} = 0.2938 \quad \text{for d} = \text{N}_2,$$

$$\frac{1}{D_{de1}} - \frac{1}{D_{df1}} = 0.3982 \quad \text{for d} = \text{CO}_2,$$

$$\frac{1}{D} - \frac{1}{D_{df1}} = 0.0546 \, \text{s} \, \text{cm}^{-2} \quad \text{for d} = \text{He},$$

$$\frac{1}{D_{ef1}} - \frac{1}{D_{df1}} = -0.0289 \quad \text{for d} = \text{N}_2,$$

$$\frac{1}{D_{ef1}} - \frac{1}{D_{df1}} = -0.0501 \quad \text{for d} = \text{CO}_2,$$

$$\frac{1}{D_{Kf}} + \frac{1}{D_{ef1}} = 0.2183 \, \text{s} \, \text{cm}^{-2}, \qquad \frac{1}{D_{ef1}} \left(\frac{1}{D_{Ke}} - \frac{1}{D_{Kf}} \right) = 0.02297 \, \text{s}^2 \, \text{cm}^{-4}, \qquad (40)$$

$$P_1 = 1.015 \times 10^5 \, \text{N} \, \text{m}^{-2}, \qquad k = 1.38 \times 10^{-23} \, \text{J} \, \text{K}, \qquad T = 1073 \, \text{K}, \qquad n_1 = \frac{P_1}{kT} = 6.855 \times 10^{18} \, \text{cm}^{-3},$$

$$w = 0.11 \, \text{cm}, \qquad S = 1.1 \, \text{cm}^2, \qquad \phi = 0.54, \qquad q = 3.2 \times 10^{-19} \, \text{C}, \qquad j_1 = 6.286 \times 10^{19} \, \text{s}^{-1},$$

$$a_{01} = 48.4 \, \text{A} \, \text{cm}^{-2}, \qquad i_1 = \frac{q j_1}{S} = 18.29 \, \text{A} \, \text{cm}^{-2}, \qquad \frac{w}{\phi q} = 6.366 \times 10^{17} \, \text{cm} \, \text{C}^{-1},$$

$$\frac{(w/\phi q)^2}{2n_1} = 2.956 \times 10^{16} \, \text{cm}^5 \, \text{C}^{-2}, \qquad \frac{w}{\phi q D_{Kf}} = 5.634 \times 10^{16},$$

$$\frac{w}{\phi q D_{ef1}} = 8.263 \times 10^{16} \, \text{s} \, \text{cm}^{-1} \, \text{C}^{-1}, \qquad \frac{w}{2\phi q n_1} \left(\frac{1}{D_{Ke}} - \frac{1}{D_{Kf}} \right) = 0.008217 \, \text{cm}^2 \, \text{s} \, \text{C}^{-1},$$

$$\frac{w}{\phi q n_1} \left(\frac{1}{D_{de1}} - \frac{1}{D_{df1}} \right) = 0.005458 \, \text{cm}^2 \, \text{s} \, \text{C}^{-1} \quad \text{for d} = \text{He},$$

$$\frac{w}{\phi q n_1} \left(\frac{1}{D_{de1}} - \frac{1}{D_{df1}} \right) = 0.02728 \, \text{cm}^2 \, \text{s} \, \text{C}^{-1} \quad \text{for d} = \text{N}_2,$$

$$\frac{w}{\phi q n_1} \left(\frac{1}{D_{de1}} - \frac{1}{D_{df1}} \right) = 0.03698 \, \text{cm}^2 \, \text{s} \, \text{C}^{-1} \quad \text{for d} = \text{CO}_2.$$

Though Eq. (38) is easy to solve exactly for τ by numerical methods, a sufficiently accurate analytical expression for τ can be obtained by approximating the exponential term by a quadratic expression,

$$\exp(c_8 \tau^2) \cong 1 + c_8 \tau^2 + \tfrac{1}{2}(c_8)^2 \tau^4. \qquad (41)$$

Then Eq. (38), or Eq. (39), becomes a quadratic equation in τ^2 and can be solved for τ in the usual manner. This quadratic equation, its solution, and its A', B' and C' coefficients are

$$A'\tau^4 + B'\tau^2 + C' = 0, \qquad \tau = \left\{ \frac{-B' \pm (B'^2 - 4A'C')^{1/2}}{2A'} \right\}^{1/2}, \qquad (42)$$

$$A' = - \left[\frac{(i_{as} w / \phi q)^2}{2n_1} \right] \left[\frac{1}{D_{ef1}} \left(\frac{1}{D_{Ke}} - \frac{1}{D_{Kf}} \right) + p_d \left(\frac{1}{D_{de1}} - \frac{1}{D_{df1}} \right) \left(\frac{1}{D_{ef1}} - \frac{1}{D_{df1}} \right) \right], \qquad (43)$$

$$B' = - \frac{i_{as} w}{\phi q} \left[\frac{1}{D_{Kf}} + \frac{1 - p_d}{D_{ef1}} + \frac{p_d}{D_{df1}} \right], \qquad C' = \left(1 - p_d - \frac{i_{as}}{i_1} - \frac{i_{as}}{a_{01}} \right) n_1. \qquad (44)$$

If we ignore the x^2 and thus the τ^4 terms in the foregoing equations by setting $A' = 0$, we find

$$\tau_{\text{linear}} = \left(\frac{-C'}{B'} \right)^{1/2}. \qquad (45)$$

Regarding the $\pm$ sign choice in Eq. (42), we note that B' is negative and C' is positive. If A' is positive, we must choose the $+$ sign because it gives the correct limit given in Eq. (45) as A' goes to zero. If A' is negative, we must choose the $-$ sign to avoid taking the square root of a negative number in Eq. (42). In Eq. (43), all expressions in round parentheses are positive, except that $(1/D_{ef1} - 1/D_{df1})$ is negative for N_2 and CO_2 diluent gases. Thus A' is negative for He, but for N_2 and CO_2 diluent gases the sign of A' depends on which term dominates in Eq. (43).

Results for the ternary gas systems are displayed in Table 2 below. There is a systematic decrease in the calculated tortuosity as the diluent concentration decreases, except for our calculations for He. Also, there is a systematic increase in calculated tortuosity as diluent molecular mass increases. In theory, the tortuosity should be independent of such experimental conditions. Although the reasons for these trends are not known, we do obtain the expected result that the τ values based on the three diluents approach each other as diluent concentration decreases.

The linear approximation to τ is accurate within a few percent. The τ values calculated by JV (the square roots of the "τ_{JV}" values reported in their paper, which are really "tortuosity factors") are larger than ours for the light He diluent gas, but comparable to ours for the heavy N_2 and CO_2 diluent gases. The variation in our "τ_{exact}" values, and the differences between our "τ_{exact}" values and the corresponding $(T_{JV})^{1/2}$ values, is greater than for the binary systems presented in Table 1. Still, all of our τ_{exact} values, centered near 2.3 and ranging from about 1.7 to 3.3, are physically reasonable and provide confidence that JV's experimental method is valid for finding tortuosity.

Plots of gas concentrations across the anode for four ternary systems under anode limiting current conditions appear in Fig. 3. All show significant increases in total gas concentration n (and thus in total pressure P) across the anode. All show decrease in diluent concentration going across the anode, because collisions with the heavier outflowing H_2O molecules have more effect than those of the lighter inflowing H_2 molecules, even though the H_2O and H_2 molecular flow rates are the same. The exponential curvature of the diluent concentrations is small but noticeable, whereas the quadratic and exponential corrections to the linear x dependences of fuel and exhaust concentrations appear insignificant.

8. Conclusions

Based on all the above results, we consider that the tortuosity for the Jiang and Virkar apparatus [1] analyzed herein is 2.3 ± 0.6. This is fairly consistent with the range of 2.5–3 found by Williford et al. [3] for modern SOFC materials, and is also within the 1–3 range that seems most physically reasonable, 1 being the limit for an extremely open and probably impractical electrode design. The apparent disagreement between our values and the tortuosity values reported by Jiang and Virkar lies in their reporting as tortuosity what is often called the tortuosity factor, which is the square of the tortuosity [2] so we can say that their actual values and ours and those of Williford et al. are in general agreement and are physically reasonable.

The more exact method presented here for calculating tortuosity, or alternatively for calculating concentration drops across the electrode if tortuosity is known, is simple enough to justify its use. Knowing concentrations at the electrode–electrolyte interfaces is essential for calculating the concentration polarization term in the voltage *vs.* current density expression. Conversely, our expressions for activation and concentration polarizations based on opposing current flows at each electrode interface with the electrolyte presented herein and derived elsewhere [8] allow us to determine the tortuosity more accurately. Such voltage calculations, together with calculations of pressure drops across electrodes and of tortuosity as presented above, provide tools for predicting performance of new SOFC designs and for analyzing performance of existing designs, both in the fuel cell and electrolysis operation modes.

Acknowledgements

References

[1] Y. Jiang, A.V. Virkar, J. Electrochem. Soc. 150 (2003) A942–A951.
[2] N. Epstein, Chem. Eng. Sci. 44 (1989) 777–779.
[3] R.E. Williford, L.A. Chick, G.D. Maupin, S.P. Simmer, J.W. Stevenson, J. Electrochem. Soc. 150 (2003) A1067–A1072.
[4] R.S. Gemmen, J. Trembly, J. Power Sources 161 (2006) 1084–1095.
[5] V.H. Schmidt, C.-L. Tsai, L.M. Lediaev, in: N.P. Bansal (Ed.), Advances in Solid Oxide Fuel Cells III, Wiley, Hoboken, NJ, 2008, pp. 129–140.
[6] F. Reif, Fundamentals of Statistical and Thermal Physics, McGraw-Hill, New York, 1965, pp. 273–287.
[7] T.K. Sherwood, R.L. Pigford, C.R. Wilke, Mass Transfer, McGraw-Hill, New York, 1975.
[8] V.H. Schmidt, Dynamic first-principles molecular-scale model for solid oxide fuel cells, in: ECS Transactions, vol. 6, issue 21, Design of Electrode Structures, E. De Castro, L. Lipp, and D. Mah (Eds.), 2008, pp. 11–24.